Journal of Materials Chemistry C

Optical Fibre-Based Sensor for the Detection of Gaseous Ammonia with Methylammonium Lead Halide Perovskite

Journal:	*Journal of Materials Chemistry C*
Manuscript ID	TC-ART-04-2018-001552.R1
Article Type:	Paper
Date Submitted by the Author:	17-May-2018

Complete List of Authors:	Ruan, Shuai; Monash University, Materials Science and Engineering Lu, Jian-Feng; Monash University, School of Chemistry; Monash university Pai, Narendra; Monash University, School of Chemistry Ebendorff-Heidepriem, Heike; Adelaide University, Institute for Photonics and Advanced Sensing Cheng, Yi-Bing; Monash University, Materials Science and Engineering Ruan, Yinlan; University of Adelaide McNeill, Christopher; Monash University, Materials Science and Engineering

Journal Name

ARTICLE

Optical Fibre-Based Sensor for the Detection of Gaseous Ammonia with Methylammonium Lead Halide Perovskite

Received 00th January 20xx,
Accepted 00th January 20xx

DOI: 10.1039/x0xx00000x

www.rsc.org/

Shuai Ruan,[ac] Jianfeng Lu,[b] Narendra Pai,[b] Heike Ebendorff-Heidepriem,[d] Yi-Bing Cheng,[ace] Yinlan Ruan,*[d] and Christopher R. McNeill*[a]

Highly fluorescent perovskite materials have attracted considerable interest for fundamental research and potential applications. In this work, we demonstrate recoverable PL quenching of methylammonium lead halide ($MAPbX_3$, where X is Cl, Br or I) upon exposure to gaseous ammonia that enables the use of hybrid perovskites in gas-sensing applications. XRD analyses confirmed that MA cations in the perovskite material were replaced by NH_3 to form $NH_4PbX_3{\cdot}MA$, thereby resulting in distinct changes in crystalline structure and consequently PL quenching. However, as a weakly coordination complex, $NH_4PbX_3{\cdot}MA$ can be easily thermally decomposed to recover the starting product $MAPbX_3$ with the release of ammonia. An in-depth understanding of the reversible chemical and structural changes of perovskite by exposing to polar molecules such as ammonia can advance the development of hybrid perovskite sensors and provide insights into mechanisms of how perovskites coordinate with polar molecules.

1. Introduction

Toxic and hazardous gas leaks such as ammonia are a significant problem for many industries. Consequences for such incidents include fatality, plant shut down and high insurance costs.[1] Meanwhile large quantities of ammonia are released in agricultural industries and used in the chemical industry, *e.g.*, for fertilizers or in refrigeration systems.[2] Thus the demand for ammonia sensing systems is increasing as gaseous ammonia is toxic even in low concentrations to many aquatic organisms.[3] In this regard, numerous materials such as metal oxides[4], sensitive organic layers[5], quantum dots[6], etc. have been extensively explored for ammonia gas sensing behaviour.

Most of the reported ammonia sensors can be classified as either electronic or optical based sensors, where the detection of ammonia is recorded by a change in either electronic or optical properties. In terms of electronic signal based sensors, the ammonia-sensitive conducting material polyaniline nanofiber was reported by Talwar *et al.*[4], with the sensor utilising changes in the conductivity of the polyaniline fibres when exposed to ammonia, with the reported sensing response found to be proportional to the ammonia gas concentration[7]. However, this film-based sensor was not reusable with a lowest detectable ammonia concentration of 25 ppm, which falls short of practical application as the odour of ammonia can even be detected by humans at concentrations >5 ppm[8]. Similarly, carbon nanotubes wrapped with polyaniline were utilised as the basis for an ammonia gas sensor[9], demonstrating a higher sensitivity (lower detection limit of 10 ppm) but with a complicated materials synthesis and time-consuming film preparation. The complex preparation also hampered the application of the poly(3-hexylthiophene)/polystyrene organic field-effect transistor based ammonia gas sensor[5]. Even though with 5 ppm detection limit, this transistor has a multilayer structure comprising PMMA/P3HT/PS/Au on Indium tin oxide (ITO) coated glass, which requires stringent spin-casting procedures. For optical based sensing, a surface plasmon resonance (SPR) based fibre sensor using poly(methyl methacrylate) (PMMA)/reduced graphene oxide nanocomposites was demonstrated[10]. The SPR spectra showed a red-shift in the resonance wavelength with increase in the concentration of gas in the chamber. Even though the probe is reusable and a SPR shift can be observed for ammonia concentration as low as 10 ppm, it showed only a 4 nm resonance wavelength shift within the detecting range from 10 to 100 ppm. This poor sensitivity thus cannot guarantee an accurate sensing. The detection of trace amounts of dissolved ammonia via the quenching of luminescence from dye molecules in a fibre-based sensor has also been demonstrated,[11] however such sensors are designed for the solution rather than gaseous detection of ammonia.

In the last few years, organic–inorganic halide perovskite based materials have been widely investigated for their various applications in photovoltaics[12], photodetectors[13], light emitting

[a] Department of Materials Science and Engineering, Wellington Road, Clayton, Victoria, 3800, Australia. E-mail: Christopher.McNeill@monash.edu.
[b] School of Chemistry, Monash University, Melbourne, Victoria, 3800, Australia.
[c] ARC Centre of Excellence in Exciton Science and Department of Materials Science and Engineering, Monash University, Melbourne, Victoria, 3800, Australia.
[d] ARC Centre of Excellence for Nanoscale BioPhotonics, Institute for Photonics and Advanced Sensing, The University of Adelaide, Adelaide, SA 5005, Australia. E-mail: Yinlan.ruan@adelaide.edu.au
[e] State Key Laboratory of Advanced Technology for Materials Synthesis and Processing, Wuhan University of Technology, Wuhan 430070, China.

† Electronic Supplementary Information (ESI) available: [XRD, SEM, TG-DTA and PL]. See DOI: 10.1039/x0xx00000x

diodes (LED)[14] and nanowire lasers[15] *etc*. The application of organic-inorganic halide perovskites as gas sensors has also been reported, albeit only by a few research groups. [16-21] Fang *et al.* [16] for example reported that the surface recombination rate (or surface trap state density) in methylammonium lead tribromide ($MAPbBr_3$) single crystals can be controlled by the physisorption of oxygen and water molecules, and indicated that as such perovskite materials may be suitable for the detection of oxygen and water vapour, especially for water vapour, which is reported can reversibly react with perovskite.[22] Xu *et al.*[20] on the other hand designed a reversible fluorescence-based humidity sensor by using $MAPbBr_3$ films. Similarly, the effects of ambient conditions on the photo-physics of perovskites were investigated by Juan *et al.*[17] through isolating oxygen and/or moisture from air. In their report, the luminescent properties of $MAPbBr_3$ were demonstrated to be strongly dependent on its atmospheric surroundings, forming oxide and hydrate species with oxygen and water molecules, respectively. Changes in electronic properties have also been observed under varied environmental atmosphere[18], with (for example) an up to a 3000-fold increase in the resistance of $MAPbI_3$-based devices observed when measured in a full oxygen atmosphere, ascribed to a trap healing mechanism originating from an oxygen-mediated filling of iodine vacancies. Apart from these effects produced by oxygen and water which are components of air, ammonia can also react with perovskite inducing a phase transformation of $MAPbI_3$, which leads to a rapid colour change from brown to colourless.[21] Even though the mechanism of the phase change is unclear, it suggests the application of perovskites for gaseous ammonia sensing.

In this work, the interaction between ammonia and $MAPbX_3$ crystals and films is studied in order to establish the feasibility of $MAPbI_xBr_{3-x}$ for application in ammonia sensors. *In situ* photoluminescence (PL) monitoring of $MAPbX_3$ crystals/films were first conducted to investigate the PL stability under continuous laser illumination. $MAPbX_3$ (where X is Cl, Br or I) crystals were then thoroughly washed with ammonia solution and then annealed in order to reveal the mechanism of the reversible phase transformation of perovskite when in contact with ammonia. SEM, XRD, PL and absorption spectra of the perovskite crystals were measured for characterisation of changes at each stage. Finally, by utilising the unique properties of organic–inorganic halide perovskites, we designed a sensitive and reusable ammonia optical fibre sensor. This was realised by the immobilization of micron-size $MAPbBr_3$ crystals on the endface of an optical fibre, which allows this sensor to have additional advantages such as probe miniaturization, ease of preparation, capability of online monitoring and remote sensing, and immunity to electromagnetic field interference over the other widely reported film-based ammonia sensors. Other common volatile solvents such as methanol, ethanol and acetone were also tested to demonstrate distinct perovskite sensor selectivity.

2. Experimental

Unless otherwise specified, all materials were purchased from Sigma-Aldrich and used as received. PbI_2 and methylammonium iodide (MAI) were dissolved in γ-butyrolactone (GBL) to prepare a 1 M $MAPbI_3$ precursor solution. For 1 M bromide and chloride based precursors, the molar ratios between MABr and $PbBr_2$, MACl and $PbCl_2$ were fixed at 1:1 and the mixed powders were dissolved in N,N-Dimethylformamide (DMF) and dimethyl sulfoxide (DMSO), respectively. These solutions were stirred and heated at 70 °C for ~ 10 min for complete dissolution and filtered with 0.2 μm filters thereafter. Polycrystalline films were prepared on plasma treated glass substrates by spin-coating precursors at 3000 rpm for 30 seconds in a N_2-filled glovebox. Following spin coating, the films were heated at 100 °C for ~ 10 min to eliminate residual solvent and promote crystallinity (Fig S4 for SEM images). Perovskite single crystals were synthesised using the previously reported Anti-solvent Vapour diffusion method.[23] Simply, by exposing precursors in a DCM atmosphere, micrometre-sized perovskite precipitates can be produced within tens of minutes, with the growth of centimetre-sized single crystals achieved after 48 hours, as demonstrated in Fig. S4.

To fabricate the functionalized optical fibre probes, $MAPbBr_3$ crystals were embedded in a polymer film at the fibre tip. Poly(methyl methacrylate) (PMMA) films were used as the host material to embed $MAPbBr_3$ owing to the favourable mechanical properties, excellent chemical stability and superior optical clarity of PMMA.[24] To prepare PMMA, PMMA powder was dissolved in dichloromethane (DCM) at a concentration of ~ 12 g/L, and the PMMA solution was then mixed with 1 M $MAPbBr_3$ precursor at a 1:1 volume ratio. Since the perovskite precursor is completely insoluble with DCM, micron-size $MAPbBr_3$ crystals instantly precipitated, and

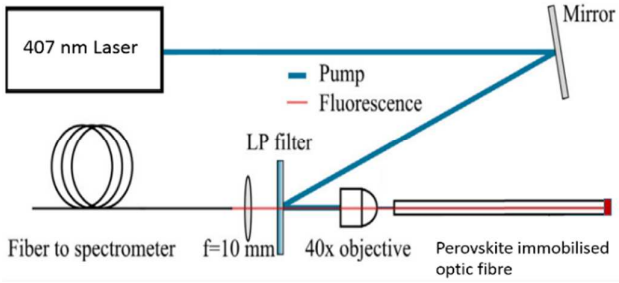

these small crystals were then immobilised on the endface of a multimode fibre through dip coating method[25]. A wet PMMA layer doped with $MAPbBr_3$ crystals was then formed by withdrawing the fibre gradually. Finally, the coated fibre end was dried at 80 °C in a drying oven for 1 hour, resulting in the formation of the layer due to solvent evaporation.

Fig. 1 Experimental setup for detection of perovskite photoluminescence using multimode optical fibres. LP filter: long pass filter.

The experimental setup for perovskite PL monitoring is shown in Fig. 1. Continuous wave (CW) light from a 407 nm semiconductor laser diode was reflected off a long pass filter (Semrock 407 nm long-pass Razor Edge Ultra steep) and

coupled into a multimode fibre with 200 μm core diameter using a 40× microscope objective. While pulsed sources can provide additional information in the form of relaxation time and fluorescence peak phase shifts, a CW laser is used as it is more practical for real-world applications being more cost-effective. The excited fluorescence signal at the fibre endface was collected in a backscattering mode, then passed through the long pass filter and recorded by a fibre coupled cooled-CCD spectrometer (Horiba Jobin-Yvon iHR320). This setup was used to detect the fibre probe's signal response towards various volatile solutions including aqueous ammonia. In order to monitor the relaxation effect of perovskite, the fibre was also be replaced by centimetre-size single crystal or polycrystalline films for PL monitoring (Fig. S5).

Scanning Electron Microscopy (SEM) images of the bulk perovskite crystals were recorded on a FEI Nova NanoSEM 450 FEG microscope using a 5 kV acceleration voltage. XRD patterns were collected with a Bruker D8 Advance diffractometer (Bragg–Brentano geometry) equipped with a Cu Kα X-ray tube operated at 40 kV and 40 mA using a step size of 0.02° and a time per step of 2 s. Thermal analyses were carried out with a STA 8000 which combines differential temperature (DTA or DSC) measurements with thermo-gravimetric (TGA).

3. Results and discussion

3.1 Perovskite PL stability under constant light illumination

It has been found that light illumination can significantly change the optical and electronic properties of perovskite crystals, such as photo-enhanced luminescence, photo-oxidation, photo-bleaching [26-31]. Since good photo-stability is a perquisite for the realisation of PL-based sensors, the perovskite PL stability under 407 nm laser illumination was first investigated. To measure the intrinsic PL characteristics of perovskite, the study of bulk single crystals is necessary as a reference material as the grain structure of perovskite thin films is known to have a strong impact on optical properties including the PL peak position (see Fig. S6), band gap position, the carrier diffusion length and the recombination pathways.[32]

Similar to previous reports[29, 33, 34], we found the PL intensity of the $MAPbI_3$ single crystal increased with increasing illumination time (Fig. 2A). Moreover, we discovered a faster PL intensity rise within the first second for $MAPbI_1Br_2$ film followed by a gradually decrease (Fig. S7). For the $MAPbBr_3$ single crystal, no slow PL rise upon illumination was observed, though a PL enhancement upon illumination at shorter timescales may still be in operation that is too fast to be recorded with the spectrometer used (Fig. 2B). Instead a slow PL decay for the $MAPbBr_3$ single crystal was observed instead. No peak shifts in the PL spectra were observed for both single crystal samples during continuous light illumination (Fig. S8). It is well known that a large density of charge carriers within perovskite crystals can be generated and sustained under continuous illumination, and the PL intensity is associated with the competition between the efficiency of radiative and non-radiative decay paths of these photo-generated carriers.[33] As for $MAPbI_3$, such PL enhancement was attributed to the passivation of trap states related to defects in the crystals.[17] Specifically, under light illumination, the traps were predominantly filled and the recombination of the photo-generated species was dominated by efficient radiative processes[29]. This defect annihilation (curing) process had been most widely proposed to explain the $MAPbI_3$ PL enhancement under illumination,[33, 35, 36] even though it has also been correlated with a redistribution of iodine in some literature[37]. Apart from photoluminescence, other optoelectronic properties such as electroluminescence[38, 39] and photoconductivity[40] have also been shown to rise slowly over time under illumination or current flow. The photo-physical processes in $MAPbI_3$ however are still far from being understood.[12, 41-43]

Furthermore, by intermittently blocking the laser irradiation via turning off a shutter in front of the laser source, we found unusual relaxation patterns for $MAPbI_3$ and $MAPbBr_3$ (Fig. 2), successive cycling of the same behaviour indicating that the single crystal did not degrade after a series of excitations. This observation also indicated that the change in PL intensity is more likely the result of a photo-physical processes rather than a photochemical degradation due to the instant change. This conclusion is at odds with some proposals that explain the $MAPbI_3$ PL change by light-driven chemical changes in the semiconductor involving ionic motion[29], or a photochemical reaction with oxygen-related species as chemical defects[33, 36]. It also should be noted that, for each cycling, the PL decrease occurs on a much longer time scale than the typical recombination lifetime of photo-generated carriers (from hundreds of nanoseconds to several microseconds). A similar PL quenching behaviour has also been observed under electric field by Deng *et al*., who demonstrated via PL imaging that the mobile ions lead to PL quenching.[44]

It is known that the defects (or quenching sites) exist not only on the surface but also in the bulk of materials[36, 45]. In our case for $MAPbBr_3$, it was found the laser induced PL quenching ratio (defined as $(I_0 - I)/I_0$, where I_0 is the initial PL intensity, I is the stabilised PL intensity) was more prominent for the centimetre-sized crystal (38 %) than the micron-sized crystal powder (28 %) and polycrystalline film (16 %) under the same illumination of 1 μW laser power (Fig. 2B, Fig. S9). If the PL quenching was related to the increased quenching sites, it can suspected that a higher defect state density was triggered by illumination of large single crystals that have less grain boundaries and dangling bonds compared with micron-size single crystal or polycrystalline film, where the crystal lattices are more randomly orientated and organised. Moreover, it seems that the defects can be re-activated due to the reversible reaction and the equilibrium between the non-active and active defects may be correlated to the intrinsic crystal structure of these single crystal or polycrystalline film.

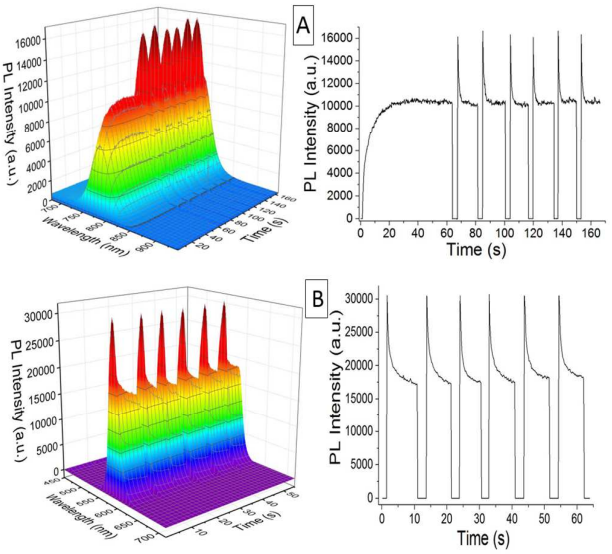

Fig. 2. Light induced PL change for $MAPbI_3$ single crystal (A), and $MAPbBr_3$ single crystal (B), whereby the laser is turned on and off consecutively. Light source: 1 μW 407 nm laser.

To investigate the impact of laser power on the relaxation effect, the PL of $MAPbBr_3$ single crystal was measured under continuous laser illumination for 15 s with varying power 0.3, 0.9 and 4.5 μW (Fig. 3A). The PL quenching ratio with increasing laser power was found as 37.4 %, 36.7 % and 36.4 %, corresponding to laser powers of 4.5, 0.9 and 0.3 μW, respectively, thus indicating the quenching dynamics is independent of laser power. Thus, we hypothesize the quenching ratio was correlated to the intrinsic properties of the sample such as defect state density or the carrier relaxation rate from defects.

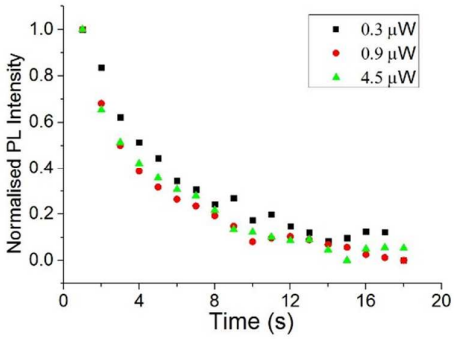

Fig. 3 The relaxation effect of $MAPbBr_3$ single crystal under continuous laser illumination with varying power.

3.2 Perovskite as ammonia sensor

The quenching of PL in $MAPbI_3$, $MAPbBr_3$ and $FAPbBr_3$ film by ammonia gas is shown in Fig. S10. As $MAPbI_3$ suffers from poor inherent stability due to relatively weak Pb-I bonds[46-49], and is susceptible to decomposition under a wide variety of environmental stimuli[50, 51] we selected $MAPbBr_3$ for ammonia sensor development. The PL of the micron-sized $MAPbBr_3$-based fibre probe decreased rapidly by 60 % even in a low ammonia concentration environment (ammonia vapour evaporating from a 0.3 wt.% ammonia solution) and recovered within 20 seconds once the ammonia source was removed (Fig. 4A). The main contributor for the PL quenching was gaseous ammonia rather than water vapour as exposure to water resulted in slight PL quenching of 32 % after 10 s while the exposure to ammonia led to a strong PL quenching of 60 % already after a short time of 2 s (Fig. S1). This difference in the response time may enable the differentiation between a water response and an ammonia response, combined with calibration of the sensor for a background response based on separately measured humidity levels. The PL quenching and recovery effect has also been observed for higher ammonia concentrations using 1 wt.% (Fig. 4B) and 3 wt.% ammonia solutions as the source(Fig. 4C) with PL quenching ratios of 80 % and 95 % respectively. However, it took longer time for the probe to recover to the initial intensity (45 s for 1 wt.% and 1300 s for 3 wt.%). Re-usability of the probe was demonstrated by initially exposing the probe to the ammonia vapour from 0.1 wt.% and then 1 wt.% ammonia solutions. The corresponding PL quenching ratio was 35 % and 80 % respectively, and the PL intensity was recovered within 45 s by removing the ammonia source (Fig. S11).

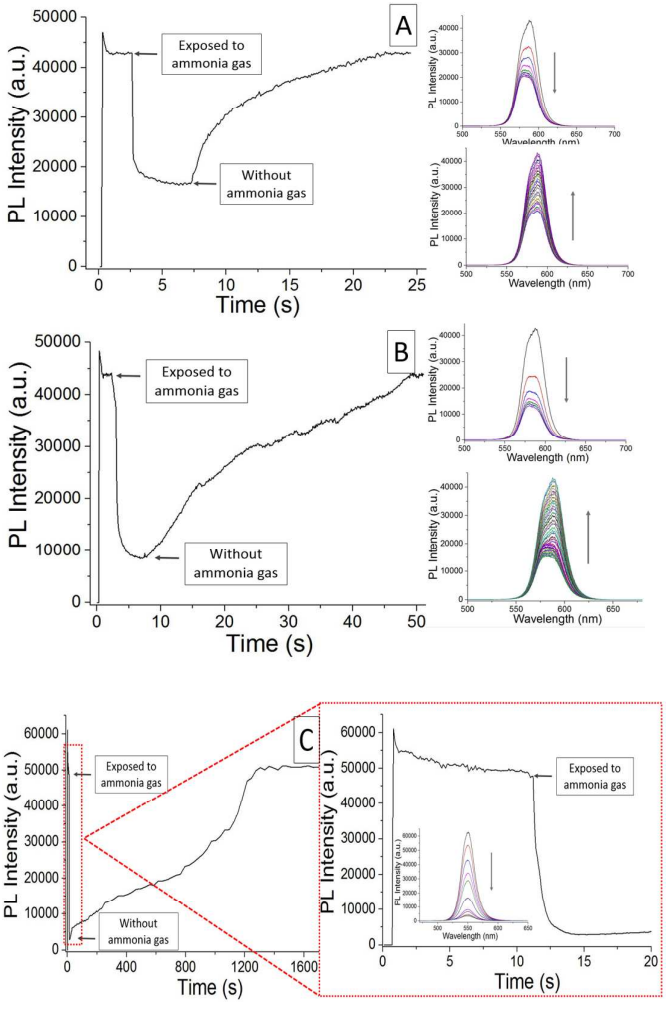

Fig. 4 PL quenching and recovery by exposing the perovskite optic fibre to ammonia vapour evaporated from 0.3 wt.%, (A), 1 wt.%, (B), and 3 wt.%, (C), ammonia solutions.

We also verified the sensor selectivity over other volatile compounds with high volatility such as water, methanol, ethanol and acetone (Fig. 5). Then sensor showed a slightly increased PL signal when exposed to organic solvents. The ratio of the PL increase was 26%, 5% and 8% for methanol, ethanol and acetone, respectively. The largest interfering signal came from water vapour as it quenched the PL intensity by 32 %, which would limit accurate ammonia detection under varied humidity conditions, more reaction details on the interaction with water can be found in the supporting material.

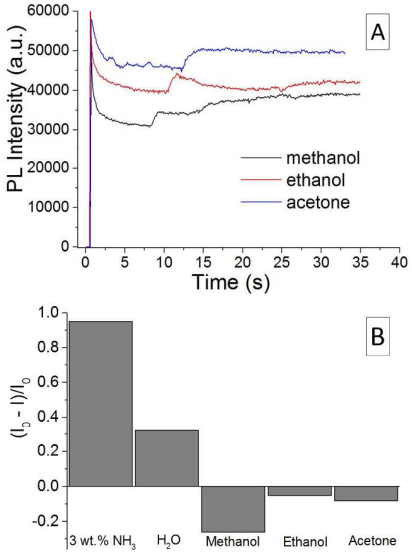

Fig. 5 *In-situ* PL intensity change (A) and quenching ratio comparison (B) of $MAPbBr_3$-based optic fibre sensor at different atmospheres.

3.3 Reaction mechanism between perovskite and ammonia

In order to gain insight into the chemical mechanism of the reaction of ammonia with perovskite, methylammonium lead halide (I, Br, Cl) single crystals thoroughly washed with 30 wt.% ammonia solution. When washing with ammonia, the colours of the crystals instantly changed to white irrespective of the halide type (Fig. S12), which indicated a phase change during ammonia wash. Note that the white appearance of the crystals here is not necessarily at odds with the observation of Zhu et al.[21] where their $MAPbI_3$ films were observed to change from brown to colourless, since the white 'colour' in our samples are due to scattering from small colourless particles. The occurrence of a phase change was further confirmed by distinct changes in the SEM morphology from cubic to rod-shaped for $MAPbBr_3$ after ammonia treatment (Fig. S13). Moreover, the original colour of the perovskite crystal was gradually recovered upon annealed at 100 °C for 5 min in the ambient air (Fig. S12). Similarly with the recovery of crystal colour, the PL of $MAPbI_3$ and $MAPbBr_3$ crystals was largely recovered after annealing, even though subtle changes in PL spectral shape are observed (Fig. 6). We note that the crystal colour is also recovered without annealing (see Figure S14) with annealing accelerating the recovery time.

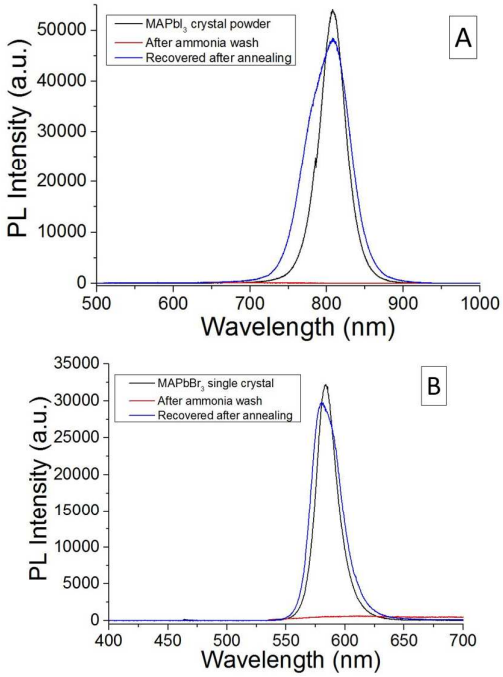

Fig. 6 PL spectra of $MAPbI_3$ (A) and $MAPbBr_3$ (B) single crystals washed with 30 wt.% ammonia solution and then annealed at 100 °C for 5 min.

Similar reversible reactions have also been reported following exposure to other amino-containing gases such as methylamine (CH_3NH_2, or "MA") and formamidine ($HN=CHNH_2$, or "FA") used to optimise the morphology of perovskite films.[52-55] Due to fast and reversible reaction, MA gas can induce defect-healing of $MAPbI_3$ thin films.[52] Similarly, MA^+ cations in $MAPbI_3$ film were rapidly replaced by FA^+ cations when exposed to FA gas to form $FAPbI_3$,[53] or displaced by NH_4^+ with exposure to ammonia gas to form NH_4PbI_3. For the latter, $MAPbI_3$ was recovered when treated with MA gas.[54, 56]

In our case, we assume that NH_4^+ (which has a smaller ionic radius to MA^+ (r_{ionic} = 1.75 Å compared with MA^+ r_{ionic} = 2.17 Å) and basic N atom with an electron lone pair in alkylamine molecules[57]) preferentially diffuses into the $[PbI_6]^{4-}$ octahedral layer to form NH_4PbI_3. This can be considered to be a redox reaction involving the reduction of MA^+ to MA and the oxidation of NH_3 into NH_4^+.Furthermore, we believe the MA molecules were still bound to the $[PbI_6]^{4-}$ structure and remained in the crystal structure, even though the bonding between MA and $[PbI_6]^{4-}$ is about an order of magnitude weaker than that between protonated MA^+ and $[PbI_6]^{4-}$ octahedral layer[56]. This process can be summarized in the following reversible equation:

$MAPbX_3(s) + NH_3(g) \leftrightarrow NH_4PbX_3{\cdot}MA(s)$

As the interaction between NH_3 and $MAPbX_3$ leads to the formation of a weakly coordinated complex, the $NH_4PbX_3{\cdot}MA$ can then easily be thermally decomposed to $MAPbX_3$ by releasing gaseous ammonia.

To confirm this proposition, XRD study was conducted to compare each stage of this reversible reaction (Fig. 7). After ammonia treatment, the diffraction pattern of $MAPbI_3$ crystal powder was dramatically changed, indicated by the disappearance of typical $MAPbI_3$ perovskite peaks at 14.2° and 28.5° indexed as (110) and (220) respectively. Instead, characteristic peaks at 9.5°, 15.7°, 23.7°, 25.2°, 37.0°, and 38.5° appear along with a host of other smaller peaks. Such a pattern does not match previous reports of the diffraction patterns of NH_4PbI_3,[54, 58] and is not easily indexed to a known crystal structure. The XRD pattern of our ammonia treated $MAPbI_3$ sample is also different to that reported by Huang et al. though in their case gas gaseous ammonia was used.[54] Upon annealing, all perovskite peaks were restored indicating that MA must remain in the structure. Thus upon exposure to ammonia, the perovskite crystal structure is changed to another crystalline form whilst retaining MA enabling the reformation of $MAPbI_3$ once ammonia is removed. For $MAPbBr_3$ and $MAPbCl_3$ striking differences in the structural change upon exposure to ammonia are observed indicating that the structural changes upon exposure to ammonia are strongly dependent upon the halide anion. For $MAPbBr_3$, the (001) peak at 15° persists throughout the ammonia wash-annealing process, while the (002) peak at 30.2° is decreased with the appearance of new peaks suggesting the formation of a new intermediate complex. All $MAPbBr_3$ peaks are restored after annealing, although some new small peaks still remain which could possibly be ascribed to a small fraction of MA leaving the crystal structure (see discussion below). For $MAPbCl_3$, all the main peaks remained unchanged throughout ammonia treatment, though again with the appearance of new peaks indicative of a $NH_4PbCl_3{\cdot}MA$ complex. $MAPbCl_3$ is also recovered after annealing with a residual impurity component. It was previously believed that the halogen anion does not have a significant impact on the overall chemical transformation process as very similar behaviour was observed for different halide anion.[56] However, through our XRD study, we found that smaller atomic size of halogen such as Cl in $MAPbCl_3$ single crystal not only leads to a contracted crystal unit cell (Fig. S15), but also facilitates a more stable perovskite structure compared with the larger unit cell of $MAPbI_3$, which showed a complete phase change after ammonia treatment.

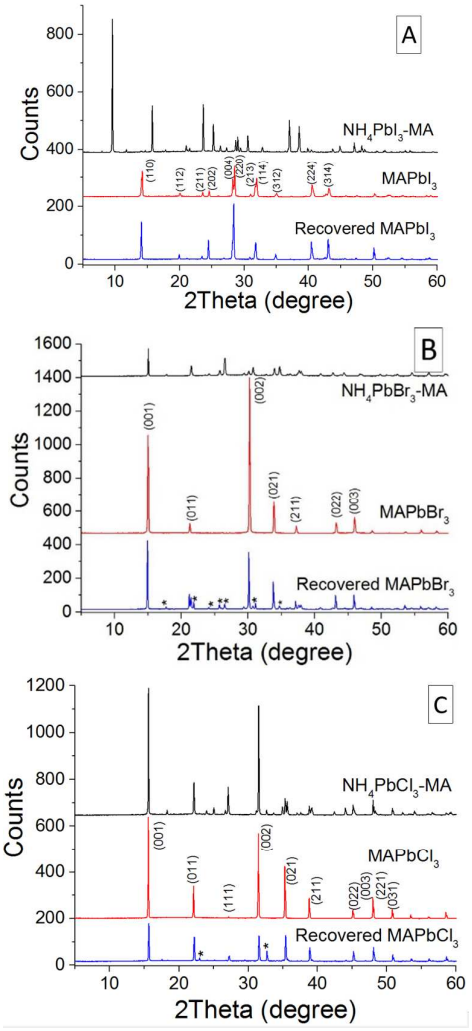

Fig. 7 XRD of $MAPbI_3$ (A), $MAPbBr_3$ (B) and $MAPbCl_3$ (C) single crystals washed with 30 wt.% ammonia solution and then annealed at 100 °C for 5 min. Peaks with "*" indicating the new peaks formed after ammonia treatment.

Furthermore, thermal gravimetric and differential thermal analysis (TG-DTA) was employed to elucidate the chemical nature of the gases released during the thermal decomposition of $NH_4PbBr_3{\cdot}MA$ (Fig. 8) (see Fig. S16 for DTA data). The TG trace for the reference $MAPbBr_3$ crystal shows two consecutive mass loss steps from 30 to 900 °C, with the former ascribed to the loss of MABr (23 wt.%) starting at 320 °C, and the latter to the inorganic $PbBr_2$ component starting at 490 °C.[59] The weight loss of MABr is consistent with its weight ratio in $MAPbBr_3$. In contrast, $NH_4PbBr_3{\cdot}MA$ showed a 2% weight loss at 30 °C, which was ascribed to ammonia sublimation considering that it is the most volatile component. Ammonia sublimation should have started before the weight loss record as the overall ammonia weight ratio in $NH_4PbBr_3{\cdot}MA$ is 3.4 wt.%. This was followed by a 1 % weight loss between 30 °C and 50 °C and a 21 % weight loss between 50 °C and 125 °C, during which range the majority of the MA was sublimated, with the MA sublimation

occurring at temperatures that are far lower than the reference sample where the MA sublimated at 320°C. This observation is consistent with what mentioned above that the bonding between MA and $[PbI_6]^{4-}$ is much weaker than that between protonated MA^+ and $[PbI_6]^{4-}$.[56] The thermally unstable MA in NH_4PbBr_3·MA was also reflected in the slight spectral change in Fig. 6 and new small XRD peaks in Fig. 7B and 7C, in which case, samples were annealed at 100 °C for 5 min after ammonia treatment. This observation may bring concerns regarding the repeatability of the fibre sensor at elevated temperature (> 50 °C). However, when considering the fully recovered PL in each sensing test in Fig. 5, the sensor works excellent at room temperature, and it is reasonable to suspect that the PMMA on the fibre tip helps to retard MA sublimation as PMMA is frequently used as a protecting layer on top of perovskite film prohibiting oxidation and hydration.[60-63]

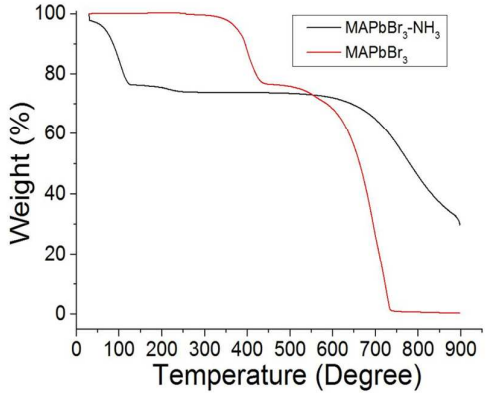

Fig. 8 The TGA weight loss comparison between $MAPbBr_3$ and NH_4PbX_3·MA.

4. Conclusions

In summary**,** we have provided here the first experimental demonstration of a perovskite-based fibre sensor for ammonia sensing. Initially, we found that continuous light illumination substantially enhance the PL intensity for methylammonium lead halide with $MAPbBr_3$ single crystal showing a much faster PL increasing rate than $MAPbI_3$. By alternate light exposure and blocking, an unusual relaxation pattern was observed for both crystals. Furthermore, the recoverable intercalation between perovskite and ammonia and the corresponding PL change allowed us to design an optical fibre based sensor which exhibited a high sensitivity towards ammonia and good selectivity over other common solvents. The in-depth study of how perovskite coordinate with ammonia also provides an insight in the reaction mechanism between perovskite and polar molecules.

Conflicts of interest

There are no conflicts to declare.

Acknowledgements

Electron microscopy access provided by the Monash University Centre for Electron Microscopy (MCEM), and XRD data provided by Monash X-Ray Platform are greatly acknowledged. The authors are also grateful to Mr. Quantao Sun and Dr. Craig Forsyth for considerable assistance in research discussions. This research was conducted by the Australia Research Council Centre of Excellence in Exciton Science (project number CE170100026) and funded by the Australian Government. This work was performed in part at the OptoFab node of the Australian National Fabrication Facility.

Notes and references

1. B. Timmer, W. Olthuis and A. Van den Berg, *Sens. Actuator B-Chem.*, 2005, **107**, 666-677.
2. B. Kuswandi, R. Andres and R. Narayanaswamy, *Analyst*, 2001, **126**, 1469-1491.
3. H. S. Mader and O. S. Wolfbeis, *Anal. Chem.*, 2010, **82**, 5002-5004.
4. V. Talwar, O. Singh and R. C. Singh, *Sens. Actuator B-Chem.*, 2014, **191**, 276-282.
5. S. Han, X. Zhuang, W. Shi, X. Yang, L. Li and J. Yu, *Sens. Actuator B-Chem.*, 2016, **225**, 10-15.
6. H. Liu, M. Li, O. Voznyy, L. Hu, Q. Fu, D. Zhou, Z. Xia, E. H. Sargent and J. Tang, *Adv. Mater.*, 2014, **26**, 2718-2724.
7. H. Yin and J. Yang, *Materials Letters*, 2011, **65**, 850-853.
8. N. R. Council and C. o. A. E. G. Levels, *Acute exposure guideline levels for selected airborne chemicals*, National Academies Press, 2009.
9. X. Tian, Q. Wang, X. Chen, W. Yang, Z. Wu, X. Xu, M. Jiang and Z. Zhou, *Applied Physics Letters*, 2014, **105**, 203109.
10. S. K. Mishra, S. N. Tripathi, V. Choudhary and B. D. Gupta, *Sens. Actuator B-Chem.*, 2014, **199**, 190-200.
11. M. Strobl, A. Walcher, T. Mayr, I. Klimant and S. M. Borisov, *Anal. Chem.*, 2017, **89**, 2859-2865.
12. M. A. Green, A. Ho-Baillie and H. J. Snaith, *Nature Photonics*, 2014, **8**, 506-514.
13. L. Dou, Y. M. Yang, J. You, Z. Hong, W.-H. Chang, G. Li and Y. Yang, *Nature communications*, 2014, **5**, 5404.
14. J. Wang, N. Wang, Y. Jin, J. Si, Z. K. Tan, H. Du, L. Cheng, X. Dai, S. Bai and H. He, *Adv. Mater.*, 2015, **27**, 2311-2316.
15. S. W. Eaton, M. Lai, N. A. Gibson, A. B. Wong, L. Dou, J. Ma, L.-W. Wang, S. R. Leone and P. Yang, *Proc. Natl. Acad. Sci. U. S. A.*, 2016, **113**, 1993-1998.
16. H.-H. Fang, S. Adjokatse, H. Wei, J. Yang, G. R. Blake, J. Huang, J. Even and M. A. Loi, *Sci. Adv.*, 2016, **2**, e1600534.
17. J. F. Galisteo-López, M. Anaya, M. Calvo and H. Míguez, *J. Phys. Chem. Lett.*, 2015, **6**, 2200-2205.
18. M. A. Stoeckel, M. Gobbi, S. Bonacchi, F. Liscio, L. Ferlauto, E. Orgiu and P. Samorì, *Adv. Mater.*, 2017, **29**.
19. C. Bao, J. Yang, W. Zhu, X. Zhou, H. Gao, F. Li, G. Fu, T. Yu and Z. Zou, *Chem. Comm.*, 2015, **51**, 15426-15429.
20. W. Xu, F. Li, Z. Cai, Y. Wang, F. Luo and X. Chen, *J. Mater. Chem. C*, 2016, **4**, 9651-9655.
21. Y. Zhao and K. Zhu, *Chem. Comm.*, 2014, **50**, 1605-1607.
22. C. Caddeo, M. I. Saba, S. Meloni, A. Filippetti and A. Mattoni, *ACS Nano*, 2017, **11**, 9183-9190.
23. D. Shi, V. Adinolfi, R. Comin, M. Yuan, E. Alarousu, A. Buin, Y. Chen, S. Hoogland, A. Rothenberger and K. Katsiev, *Science*, 2015, **347**, 519-522.

24. R. Kostecki, H. Ebendorff-Heidepriem, S. Afshar, G. McAdam, C. Davis and T. M. Monro, *Opt Mater Express*, 2014, **4**, 1515-1525.
25. S. Sekimoto, H. Nakagawa, S. Okazaki, K. Fukuda, S. Asakura, T. Shigemori and S. Takahashi, *Sens. Actuator B-Chem.*, 2000, **66**, 142-145.
26. S. Chen, X. Wen, S. Huang, F. Huang, Y. B. Cheng, M. Green and A. Ho-Baillie, *Solar RRL*, 2017, **1**.
27. J. S. Manser and P. V. Kamat, *Nat. Photonics*, 2014, **8**, 737-743.
28. C. Wehrenfennig, G. E. Eperon, M. B. Johnston, H. J. Snaith and L. M. Herz, *Adv. Mater.*, 2014, **26**, 1584-1589.
29. S. D. Stranks, V. M. Burlakov, T. Leijtens, J. M. Ball, A. Goriely and H. J. Snaith, *Phys. Rev. Appl.*, 2014, **2**, 034007.
30. M. Ghanassi, M. Schanne ‐ Klein, F. Hache, A. Ekimov, D. Ricard and C. Flytzanis, *Appl. Phys. Lett.*, 1993, **62**, 78-80.
31. C. Wehrenfennig, M. Liu, H. J. Snaith, M. B. Johnston and L. M. Herz, *Energy Environ. Sci.*, 2014, **7**, 2269-2275.
32. H. Diab, G. Trippé-Allard, F. Lédée, K. Jemli, C. Vilar, G. Bouchez, V. L. Jacques, A. Tejeda, J.-S. Lauret and E. Deleporte, *arXiv preprint arXiv:1606.01729*, 2016.
33. Y. Tian, M. Peter, E. Unger, M. Abdellah, K. Zheng, T. Pullerits, A. Yartsev, V. Sundström and I. G. Scheblykin, *Phys. Chem. Chem. Phys.*, 2015, **17**, 24978-24987.
34. Y. Tian, A. Merdasa, M. Peter, M. Abdellah, K. Zheng, C. S. Ponseca Jr, T. n. Pullerits, A. Yartsev, V. Sundström and I. G. Scheblykin, *Nano Lett.*, 2015, **15**, 1603-1608.
35. Y. Yamada, M. Endo, A. Wakamiya and Y. Kanemitsu, *J. Phys. Chem. Lett.*, 2015, **6**, 482-486.
36. Y. Tian, A. Merdasa, E. Unger, M. Abdellah, K. Zheng, S. McKibbin, A. Mikkelsen, T. n. Pullerits, A. Yartsev and V. Sundström, *J. Phys. Chem. Lett.*, 2015, **6**, 4171-4177.
37. W. Zhang, V. M. Burlakov, D. J. Graham, T. Leijtens, A. Osherov, V. Bulović, H. J. Snaith, D. S. Ginger and S. D. Stranks, *Nat. Commun.*, 2016, **7**, ncomms11683.
38. K. Wojciechowski, S. D. Stranks, A. Abate, G. Sadoughi, A. Sadhanala, N. Kopidakis, G. Rumbles, C.-Z. Li, R. H. Friend and A. K.-Y. Jen, *ACS Nano*, 2014, **8**, 12701-12709.
39. W. Tress, N. Marinova, T. Moehl, S. M. Zakeeruddin, M. K. Nazeeruddin and M. Grätzel, *Energy Environ. Sci.*, 2015, **8**, 995-1004.
40. R. Gottesman, E. Haltzi, L. Gouda, S. Tirosh, Y. Bouhadana, A. Zaban, E. Mosconi and F. De Angelis, *J. Phys. Chem. Lett.*, 2014, **5**, 2662-2669.
41. T. C. Sum and N. Mathews, *Energy Environ. Sci.*, 2014, **7**, 2518-2534.
42. J. A. Christians, J. S. Manser and P. V. Kamat, *J. Phys. Chem. Lett.*, 2015, **6**, 2086-2095.
43. V. D'Innocenzo, G. Grancini, M. J. Alcocer, A. R. S. Kandada, S. D. Stranks, M. M. Lee, G. Lanzani, H. J. Snaith and A. Petrozza, *Nat. Commun.*, 2014, **5**, 3586.
44. X. Deng, X. Wen, C. F. J. Lau, T. Young, J. Yun, M. A. Green, S. Huang and A. W. Ho-Baillie, *J. Mater. Chem. C*, 2016, **4**, 9060-9068.
45. B. Valeur and M. N. Berberan-Santos, *Molecular Fluorescence: Principles and Applications*, John Wiley & Sons, 2012.
46. Y. Rong, L. Liu, A. Mei, X. Li and H. Han, *Adv. Energy Mater.*, 2015, **5**.
47. G. Niu, X. Guo and L. Wang, *J. Mater. Chem. A*, 2015, **3**, 8970-8980.
48. T. A. Berhe, W.-N. Su, C.-H. Chen, C.-J. Pan, J.-H. Cheng, H.-M. Chen, M.-C. Tsai, L.-Y. Chen, A. A. Dubale and B.-J. Hwang, *Energy Environ. Sci.*, 2016, **9**, 323-356.
49. J. S. Manser, M. I. Saidaminov, J. A. Christians, O. M. Bakr and P. V. Kamat, *Acc. Chem. Res.*, 2016, **49**, 330-338.
50. C. Eames, J. M. Frost, P. R. Barnes, B. C. O'regan, A. Walsh and M. S. Islam, *Nat. Commun.*, 2015, **6**, 7497.
51. S. Meloni, T. Moehl, W. Tress, M. Franckevičius, M. Saliba, Y. H. Lee, P. Gao, M. K. Nazeeruddin, S. M. Zakeeruddin and U. Rothlisberger, *Nat. Commun.*, 2016, **7**, 10334.
52. Z. Zhou, Z. Wang, Y. Zhou, S. Pang, D. Wang, H. Xu, Z. Liu, N. P. Padture and G. Cui, *Angew. Chem. Int. Ed*, 2015, **54**, 9705-9709.
53. Y. Zhou, M. Yang, S. Pang, K. Zhu and N. P. Padture, *J. Am. Chem. Soc.*, 2016, **138**, 5535-5538.
54. W. Huang, J. S. Manser, S. Sadhu, P. V. Kamat and S. Ptasinska, *J. Phys. Chem. Lett.*, 2016, **7**, 5068-5073.
55. S. Pang, Y. Zhou, Z. Wang, M. Yang, A. R. Krause, Z. Zhou, K. Zhu, N. P. Padture and G. Cui, *J. Am. Chem. Soc.*, 2016, **138**, 750-753.
56. Y. Zong, Y. Zhou, M. Ju, H. F. Garces, A. R. Krause, F. Ji, G. Cui, X. C. Zeng, N. P. Padture and S. Pang, *Angew. Chem. Int. Ed*, 2016, **55**, 14723-14727.
57. R. Warren and W. Liang, *J. Phys. Condens. Matter*, 1993, **5**, 6407.
58. Z. Zhou, S. Pang, F. Ji, B. Zhang and G. Cui, *Chem. Comm.*, 2016, **52**, 3828-3831.
59. G. Nagabhushana, R. Shivaramaiah and A. Navrotsky, *Proc. Natl. Acad. Sci. U. S. A.*, 2016, **113**, 7717-7721.
60. H. Yu, F. Wang, F. Xie, W. Li, J. Chen and N. Zhao, *Adv. Funct. Mater.*, 2014, **24**, 7102-7108.
61. S. D. Stranks, G. E. Eperon, G. Grancini, C. Menelaou, M. J. Alcocer, T. Leijtens, L. M. Herz, A. Petrozza and H. J. Snaith, *Science*, 2013, **342**, 341-344.
62. D. Bi, C. Yi, J. Luo, J.-D. Décoppet, F. Zhang, S. M. Zakeeruddin, X. Li, A. Hagfeldt and M. Grätzel, *Nat. Energy*, 2016, **1**, 16142.
63. M. Hirasawa, T. Ishihara, T. Goto, K. Uchida and N. Miura, *Physica B: Condens. Matter*, 1994, **201**, 427-430.

A novel optical fibre-based sensor utilising photoluminescence quenching in methylammonium lead halides upon exposure to ammonia is demonstrated.